p-Aryl-Substituted Iminopyridine Chromium Complexes as Precatalysts for Ethylene Polymerization: The Question of the Physical Oxidation State Examined by Experimental

Para-Aryl–Substituted Iminopyridine Chromium Complexes as Precatalysts for Ethylene Polymerization: The Question of the Physical Oxidation State by Experimental and Density Functional Study in the Absence of Structural Data

Journal:	*Organometallics*
Manuscript ID	om-2024-00187m.R1
Manuscript Type:	Article
Date Submitted by the Author:	n/a
Complete List of Authors:	Zanchin, Giorgia; Istituto per lo Studio delle Macromolecole Consiglio Nazionale delle Ricerche, Amodio, Alessia; University of Turin Piovano, Alessandro; Politecnico di Torino, Chemistry Guiotto, Virginia; Università di Torino, Dipartimento di Chimica Leone, Giuseppe; Istituto di Scienze e Tecnologie Chimiche "Giulio Natta", Falivene, Laura; University of Salerno Department of Chemistry and Biology Groppo, Elena; University of Turin, Chemistry

Para-Aryl–Substituted Iminopyridine Chromium Complexes as Precatalysts for Ethylene Polymerization: The Question of the Physical Oxidation State by Experimental and Density Functional Study in the Absence of Structural Data

Giorgia Zanchin,[a,§] Alessia Amodio,[b] Alessandro Piovano,[b,ᶻ] Virginia Guiotto,[b] Giuseppe Leone,[a,*] Laura Falivene,[c,*] and Elena Groppo[b,*]

[a] CNR-Istituto di Scienze e Tecnologie Chimiche "Giulio Natta" (SCITEC), via A. Corti 12, I-20133 Milano, Italy.

[b] Department of Chemistry, NIS Interdepartmental Research Center and INSTM Reference Center, University of Torino, via G. Quarello 15/A, I-10135 Torino, Italy.

[c] Dipartimento di Chimica e Biologia, Università di Salerno, Via Papa Paolo Giovanni II, 84100 Fisciano, SA, Italy.

[§] *present address:* Centrocot SpA, piazza Sant'Anna 2, I-21052 Busto Arsizio, Italy.

[ᶻ] *present address:* GAME Lab (GISEL-INSTM associated), Department of Applied Science and Technology, Polytechnic of Torino, Corso Duca Degli Abruzzi 24, I-10129 Torino, Italy.

corresponding authors

giuseppe.leone@scitec.cnr.it (G.L.)

lafalivene@unisa.it (L.F.)

elena.groppo@unito.it (E.G.)

---

graphical abstract

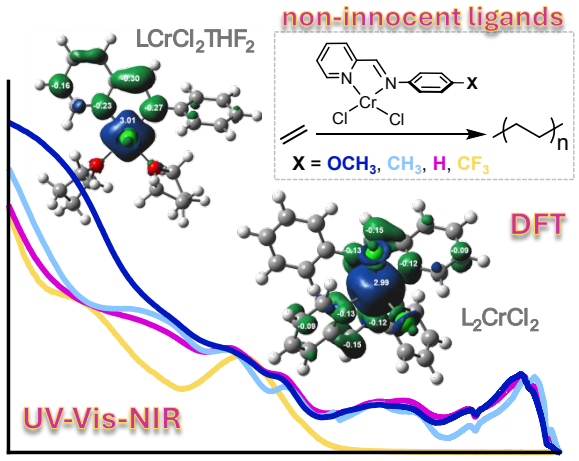

Abstract

Recent investigations into iminopyridine (ImPy) chromium complexes have unveiled their potential as precatalysts for the polymerization of various (di)olefins (*Organometallics* **2018**, *37*, 4827−4840). The occurrence of a concerted Cr−to−ligand electron transfer, with the ImPy in the monoanionic radical $(L^{\bullet})^{-}$ state and the Cr in a *physical* trivalent oxidation state, was proved to be fundamental to facilitate the polymerization of ethylene catalyzed by the complex with the unsubstituted aldimine ligand, **Cr-*p*H** (X = H). In the absence of structural data, we embarked on a detailed study by combining UV−Vis−NIR spectroscopy with density functional theory (DFT) calculations to elucidate the structural and electronic features driving this electron transfer in **Cr-*p*H**. Our findings reveal that the Cr−to−L electron transfer is facilitated either by the presence of two THF molecules in the metal's coordination sphere in the mono-ligated form, or by the formation of a bis-ligated species. The experimental UV−Vis−NIR spectrum of **Cr-*p*H**, coupled with ESI-MS results, indicates the coexistence of multiple species. Successively, we enlarged the library of chromium complexes competent in the insertion polymerization of ethylene by appending different substituents (*i.e.*, CH_3, OCH_3 and CF_3) at the *para*-*N*-aryl 4-position on the aniline moiety, in order to modulate the electron donating capability of the ligand without significantly modifying the steric bulk around the metal. While **Cr-*p*CH$_3$** and **Cr-*p*OCH$_3$** display electronic features analogous to those of **Cr-*p*H**, indicative of an equilibrium between different species, **Cr-*p*CF$_3$** stands out as an exception, likely containing only mono-ligated species with two THF co-ligands. All the complexes demonstrated activity in ethylene polymerization, with activity increasing alongside the electron withdrawing ability of the ligand substituent. Notably, **Cr-*p*CF$_3$** emerged as the most active catalyst, producing ultra-high-molecular-weight poly(ethylene) (UHMWPE) with unimodal and narrow molecular weight distribution event at 40 °C.

1. Introduction

Since the commercialization of Ziegler−Natta and Phillips catalysts to produce poly(ethylene)s (PEs) in the 1950s,[1,2] many transition metal−catalyzed coordination−insertion polymerization processes have been developed for the synthesis of various PE grades.[3−9] Today, PE has become one of the most common synthetic plastic, which has transformed modern-day life, supplying valuable, economical, and sometimes unreplaceable alternatives to wood, glass and metals. Although the majority of PE is industrially produced through heterogeneous catalysts, the development of homogeneous catalysts is of pivotal significance for mechanistic understanding and may offer promising opportunities for the fabrication of high−performance, functional, and durable PEs,[10−15] which can replace other polymers in the plastic value chain, giving access to more easily recyclable all-polyolefin composite materials.[16]

Typically, the reactivity of a transition metal catalyst is determined by the redox reactions taking place at the metal centre, which in turn is strongly affected by the ligands, that pull or push electron density and govern the steric environment around the metal. Generally, such ligands are spectators (or "innocent"): their participation to the chemistry of the metal complex is exclusively ancillary. However, while still less common, a certain number of ligands may reversibly accept electron(s) during the redox events occurring at the metal center,[17,18] thereby playing a "non-innocent" role. This feature endows transition metal complexes with unique redox properties and has proved to be useful for catalyst design.[19−21] Indeed, the combination of transition metals with redox non-innocent ligands has the potential to access catalysts where the individual components combine synergistically to give rise to unique and unexpected reactivity. Among the electron-accepting π-systems, ImPys are talented in storing multiple reducing equivalents, thereby granting many compounds of first-row transition metals to act as competent catalysts in reactions involving concerted 2e$^-$ chemistry. Studies by Wieghardt revealed the ability of ImPys in metal complexes to accept one or two electrons to form monoanionic π-radical $(L^{\bullet})^{1-}$ or the doubly reduced dianion $(L^{red})^{2-}$ ligands, respectively (Scheme 1).[22]

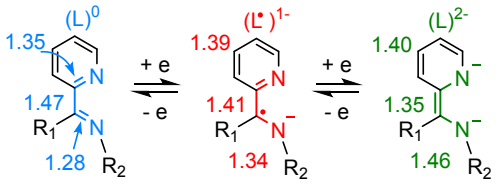

Scheme 1. Different Redox States of the ImPy ligand with their characteristic bond distances (in Å).[22]

ImPys have been reported to efficiently coordinate various transition metals and the resultant compounds have proved to be excellent (pre)catalysts for the (co)polymerization of ethylene,[23−28] copolymerization of CO with vinyl arenes,[29,30] and polymerization of cyclic olefins,[31] and 1,3-dienes.[32−36] Nevertheless, only very few examples of ImPy−Cr complexes have been published so

far.[37–41] Although many of them have been accepted as bearing non-innocent ligands, an accurate assignment of the electronic structure and definition of the metal oxidation state is still lacking. Besides, most of these chromium complexes are fruitful precatalysts for the oligomerization of ethylene, but not for its polymerization.[42]

A recent study by some of us has attempted to address the chemistry of ImPy−Cr complexes by examining a series differing in the nature of the starting chromium salt (either Cr(II) or Cr(III) chlorides), and in the type of substituents both at the iminic carbon and at the *ortho*−aryl positions (Chart 1A). While the ligands feature similar electron-accepting properties, the chemistry of the chromium complexes results very different. Remarkably, when starting from the $CrCl_2$ salt, the *ortho*−aryl ligand substituents play a key role in stabilizing the Cr oxidation state +2, while the complex with the unsubstituted aniline **L*p*H** (hereafter labeled as **Cr-*p*H**) actually contains Cr +3 species coupled to the ImPy−centered π-radical monoanion $(\mathbf{L}p\mathbf{H}^{\bullet})^{-}$. As a consequence of the occurrence of this concerted Cr−to−L electron transfer, only **Cr-*p*H** efficiently catalyzed the polymerization of ethylene to fabricate high molecular weight (MW) PEs,[38] and ultra-high molecular weight (UHMWPE).[37]

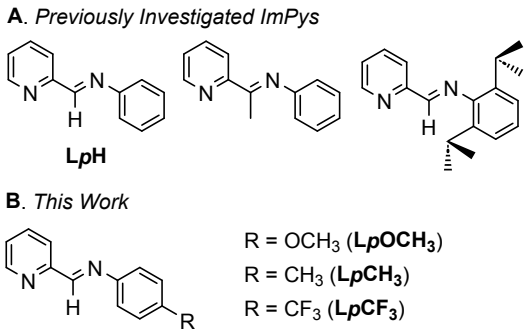

Chart 1. (A) ImPys previously studied by some of us and (B) ImPys investigated in this work.

As part of our ongoing efforts in developing Cr catalysts effective in the polymerization of ethylene, herein we investigate in detail which are the structural features leading to the Cr−to−L electron transfer, we define the chromium *real* oxidation state, and we assign the electronic structure of **Cr-*p*H** by combining UV−Vis−NIR spectroscopy with DFT calculations. Moreover, we enlarged the library of ImPy−Cr complexes. Having already demonstrated that *ortho* substitution is detrimental to catalysis and the electron transfer does not occur, we appended substituents at the *para*-aryl 4-position on the aniline moiety in order to affect the electron donating ligand capability, without modifying meaningfully the steric hindrance around the metal (Chart 1B). In the absence of structural characterization, which is a quite common situation when dealing with flexible and poorly substituted ligands, the electronic and vibrational properties of the *para*-substituted Cr complexes are investigated by UV−Vis−NIR and IR spectroscopies complemented by DFT calculations.

2. Experimental

2.1. Materials and Methods

Manipulations of air- and/or moisture-sensitive materials were carried out under an inert atmosphere, using a dual vacuum/nitrogen line and standard Schlenk-line techniques with oven-dried glassware. Nitrogen and ethylene were purified by passage over columns of $CaCl_2$, molecular sieves, and BTS catalysts. THF (Merck, ≥99.9%) was refluxed over Na/benzophenone alloy for 8 h and then distilled and stored over molecular sieves. Toluene (Merck, >99.5%) was refluxed over Na for 8 h and then distilled and stored over molecular sieves. Pentane (Merck, >99%) was refluxed over Na/K alloy for 8 h and then distilled and stored over molecular sieves. Dichloromethane (Merck, ≥99.9%) was dried by stirring over CaH_2 in an inert atmosphere for 8 h, distilled, and stored over 5Å molecular sieves away from bright light. Methylaluminoxane (MAO - Merck, 7 wt% solution in toluene), $CrCl_2$ (Merck 99.99%), 2-Pyridine carboxaldehyde (Merck), deuterated solvent for NMR measurements ($C_2D_2Cl_4$) (Merck, >99.5% atom D), and all the anilines (Merck) were used as received.

2.2. Synthesis of the ImPy ligands (L*p*R)

The target ImPys were synthesized by the condensation reaction of the 2-pyridine carboxaldehyde with the desired aniline according to the literature procedures (Scheme 2).[32,38] The synthesis of the prototype ligand **L*p*H** is reported in reference 38. Briefly, the reaction was carried out in an oven dried, nitrogen purged, Schlenk fitted with a nitrogen inlet and a septum. A mixture of 2-pyridinecarboxaldehyde (1 mmol) and 1 molar equivalent of the respective aniline derivatives were dissolved in anhydrous solvent (10 mL) in the presence of 10 grams of 5 Å molecular sieves. The mixture was stirred and heated to reflux for 8−12 h; subsequently the resultant solutions were filtered to remove the molecular sieves and evaporated in vacuo to afford the crude products. When necessary, ligands were purified by recrystallization or flash silica gel column chromatography.

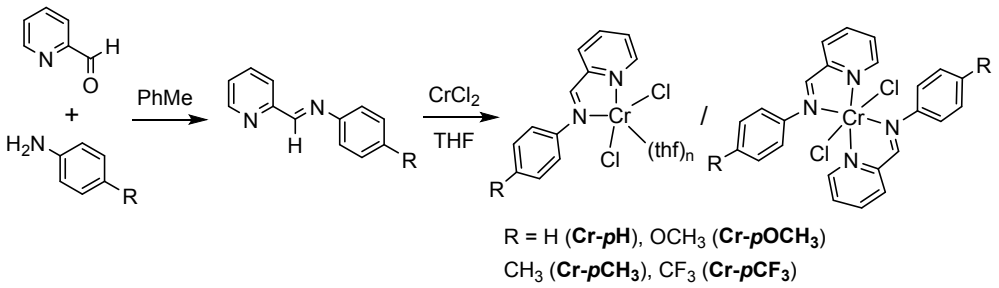

Scheme 2. Synthesis of the ImPy ligands (**L*p*R**) and corresponding chromium complexes (**Cr-*p*R**) as major species detected by ESI-MS [n = 0 (**M0**), 1 (**M1**), 2 (**M2**)].

N-(pyridin-2-ylmethylene)-4-(trifluoromethyl)aniline (**L*p*CF$_3$**). 2-pyridine carboxaldehyde (1 mmol) and *p*-(tetrafluoro)methylaniline (1 mmol) in anhydrous toluene were refluxed for 3 h. **L*p*CF$_3$** was

obtained by recrystallization from hexane to give white crystals. Yield: 66%; ^{1}H NMR (400 MHz, $CDCl_3$): δ 8.80 (d, 1H), 8.64 (s, 1H), 8.26 (d, 1H), 7.91 (t, 1H), 7.74 (m, 2H), 7.48 (t, 1H), 7.39 (m, 2H). These signals agree with those reported in the literature.[43]

4-methyl-N-(pyridin-2-ylmethylene)aniline (**L*p*CH$_3$**). 2-pyridine carboxaldehyde (1 mmol) and *p*-toluidine (1 mmol) were mixed in anhydrous methanol for 3 h. **L*p*CH$_3$** was obtained by recrystallization from hexane to give yellow crystals. Yield: 70%; ^{1}H NMR (400 MHz, $CDCl_3$): δ 8.75 (d, 1H), 8.66 (s, 1H), 8.24 (d, 1H), 7.85 (t, 1H), 7.40 (t, 1H), 7.24 (s, 4H), 2.43 (s, 3H). These signals agree with those reported in the literature.[44]

4-methoxy-N-(pyridin-2-ylmethylene)aniline (**L*p*OCH$_3$**). 2-pyridine carboxaldehyde (1 mmol) and *p*-anisidine (1 mmol) were mixed in anhydrous dichloromethane at room temperature for 16 h. **L*p*OCH$_3$** was obtained by recrystallization from hexane to give light yellow crystals. Yield: 70%; ^{1}H NMR (400 MHz, $CDCl_3$): δ 8.70 (d, 1H), 8.63 (s, 1H), 8.18 (d, 1H), 7.8 (t, 1H), 7.34 (m, 3H), 6.69 (d, 2H), 3.84 (s, 3H). These signals agree with those reported in the literature.[45]

2.3. Synthesis of the ImPy−Cr Complexes (Cr-*p*R)

The **L*p*R** ligands were then reacted in stoichiometric amount with $CrCl_2$ in THF at room temperature to produce the corresponding Cr complexes, which rapidly precipitated from an initially clear solution (Scheme 2). The solids were isolated in high yield, from 86 to 99%. The complexes have colours from green brownish to deep green and are highly air and moisture sensitive, thus requiring manipulation under strictly inert conditions.

Dichloro(N-(pyridin-2-ylmethylene)aniline) Chromium Dichloride Complex (Cr-pH). Dark brown solid. Yield (based on $CrCl_2$): 92%. Anal. Calcd for $LCrCl_2$ ($C_{12}H_{10}Cl_2CrN_2$): C, 47.24; H, 3.30; N, 9.18. Found: C, 49.68; H, 4.17; N, 7.25. ESI-MS: *m*/*z* 303.98 $[LCrCl_2]^+$, 344.98 $[LCrCl_2{\cdot}CH_3CN]^+$, 386.05 $[LCrCl_2{\cdot}2CH_3CN]^+$, 486.05 $[L_2CrCl_2]^+$.

Dichloro[N-(pyridin-2-ylmethylene)-4-(trifluoromethyl)aniline] Chromium Dichloride Complex (**Cr-*p*CF$_3$**). Green solid. Yield (based on $CrCl_2$): 86%. Anal. Calcd for $LCrCl_2$ ($C_{13}H_9Cl_2CrF_3N_2$: C, 41.85; H, 2.43; N, 7.51. Found: C, 42.04; H, 3.19; N, 7.35. ESI-MS: *m*/*z* 371.94 $[LCrCl_2]^+$, 412.05 $[LCrCl_2{\cdot}CH_3CN]^+$, 454.04 $[LCrCl_2{\cdot}2CH_3CN]^+$, 622.12 $[L_2CrCl_2]^+$.

Dichloro[4-methyl-N-(pyridin-2-ylmethylene)aniline] Chromium Dichloride Complex (**Cr-*p*CH$_3$**). Dark green solid. Yield (based on $CrCl_2$): 90%. Anal. Calcd for $LCrCl_2$ ($C_{13}H_{12}Cl_2CrN_2$): C, 48.92; H, 3.79; N, 8.78. Found: C, 47.99; H, 4.47; N, 8.33. ESI-MS: *m*/*z* 317.96 $[LCrCl_2]^+$, 360.98 $[LCrCl_2{\cdot}CH_3CN]^+$, 402.05 $[LCrCl_2{\cdot}2CH_3CN]^+$, 514.10 $[L_2CrCl_2]^+$.

Dichloro[4-methoxy-N-(pyridin-2-ylmethylene)aniline] Chromium Dichloride Complex (**Cr-*p*OCH$_3$**). Dark green solid. Yield (based on $CrCl_2$): 99%. Anal. Calcd for $LCrCl_2$ ($C_{13}H_{12}Cl_2CrN_2O$):

C, 46.59; H, 3.61; N, 8.36. Found: C, 46.54; H, 4.22; N, 8.18. ESI-MS: *m*/*z* 333.96 $[LCrCl_2]^+$, 374.0 $[LCrCl_2{\cdot}CH_3CN]^+$, 416.04 $[LCrCl_2{\cdot}2CH_3CN]^+$, 546.11 $[L_2CrCl_2]^+$.

Deviations in the experimental elemental analysis from calculated values can arise from a variety of factors including solvent inclusion, moisture adsorption, coordination variability, oxidation or reduction, and incomplete combustion that cause inaccurate results.[38,46] Besides, even more importantly, and as it will be discussed later, the investigated chromium complexes exist in different structural forms. These different forms can have varying elemental compositions due to differences in coordination environments and inclusion of solvent molecules. Unfortunately, despite numerous attempts, the synthesized complexes were recalcitrant in forming single crystals suitable for a structural characterization by X-ray diffraction.

2.3 Polymerization

Polymerization of ethylene was carried out in a 50 mL round-bottomed Schlenk flask at 20 °C (and for **Cr-*p*CF$_3$** also at 40 and 60 °C). Beyond this reaction temperature, the chain transfer reactions became significantly faster than the chain propagation reactions, indicating a certain instability at higher temperatures. Prior to the start of polymerization, the reactor was heated to 110 °C under vacuum for 1 h and back-filled with nitrogen. The reactor was charged at room temperature with toluene and MAO cocatalyst in that order. After thermal equilibration at the desired temperature, the solution was degassed, and ethylene was added until saturation. Polymerization was started by adding a CH_2Cl_2 solution (2 mg mL^{-1}) of the chromium complex via syringe under a continuous flow of ethylene (1.01 bar). Polymerizations were stopped with methanol containing a small amount of hydrochloric acid; the precipitated polymers were collected by filtration, repeatedly washed with fresh methanol, and finally dried under vacuum at room temperature to constant weight. In all of the reactions investigated, no polymerization activity was observed in the absence of the chromium source.

2.4. Characterization

Elemental analysis was performed using a Thermo Fisher Scientific FlashEA 1112 instrument, calibrated with 2,5-Bis(5-tert-butyl-benzoxazol-2-yl)thiophene (BBOT) as the standard. About 1.7–2.0 mg of sample has been used for each measurement. The samples were loaded together with the V_2O_5 catalyst (in a 1:1 ratio) into tin capsules and then immediately inserted into the instrument for the measurement, one at a time, in order to avoid contamination by moisture. Three repetitions were performed, and the results were averaged. The mass spectra were recorded using a Micromass Quattromicro™ API triple quadrupole mass spectrometer (Waters) and the data were acquired using Masslynx software. Samples were dissolved in CH_3CN. Infusion into the mass spectrometer was

performed by the built-in syringe pump at a flow rate of 10 μl min^{-1}. Nitrogen was used as desolvation and nebulization gas. The source temperature was kept at 120 °C while the desolvation temperature was kept at 150 °C. The ESI capillary voltage was maintained at 4 kV while the cone voltage at 60 V. IR spectra of the ligands and of the complexes in powder form were acquired in attenuated total reflectance (ATR) mode, at a resolution of 2 cm^{-1}, using a Bruker Alpha spectrophotometer equipped with a diamond ATR crystal, which was placed inside a N_2-filled glovebox to avoid sample contamination by moisture. UV−Vis−NIR spectra of the complexes in the powder form were collected using a Cary5000 spectrophotometer equipped with a reflectance sphere. The samples were diluted with Teflon powder in the glovebox, inserted into a home-made cell with windows in optical quartz (Suprasil) and closed with teflon plugs. The spectra were collected in reflectance (R%) and converted in Kubelka-Munk function F(R) afterwards. ATR–IR spectra of the polymers were recorded at room temperature in the 4000–600 cm^{-1} range with a resolution of 4 cm^{-1} using a Perkin-Elmer Spectrum Two spectrometer. The average molecular weight (M_w) and molecular weight distribution (M_w/M_n) were obtained by a high-temperature Waters GPCV2000 size exclusion chromatography (SEC) system using an online refractometer detector. The experimental conditions consisted of three PL Gel Olexis columns, o-dichlorobenzene as the mobile phase, 0.8 mL min^{-1} flow rate, and 145 °C temperature. The calibration of the SEC system was constructed using 18 narrow M_w/M_n PS standards with *M*w values ranging from 162 to 5.6×10^6 g mol^{-1}. For SEC analysis, about 12 mg of the polymer was dissolved in 5 mL of *ortho*-dichlorobenzene. Differential scanning calorimetry (DSC) measurements were performed with a Mettler DSC822 operating in a N_2 atmosphere. The sample (5 mg) was placed in a sealed aluminum pan, and the measurement was performed from −70 to 180 °C using a heating and cooling rate of 10 °C min^{-1}.

3. Theoretical Methods

Geometry optimizations were performed using the Gaussian 09 program (Revision D.01),[47] the B3LYP functional[48−50] and the SVP[51] basis set on all atoms except for chromium, which was modelled with the SDD basis set.[52,53] Frequency calculations at the same level of theory confirmed that the optimized structures were a minimum on the potential energy surface. Single point calculations were performed using the B3LYP functional and the triple-ζ plus one polarization function basis set proposed by Ahlrichs (TZVP keyword in Gaussian) on all atoms except for chromium which was modelled with the SDD basis set. Final energies are B3LYP/TZVP//B3LYP/SVP electronic energies corrected with ZPEs, thermal energies, and entropy effects calculated at 298 K using the B3LYP/SVP method.

Excited-state calculations were performed using time-dependent DFT (TDDFT). Excited state energies were calculated for the 30 lowest triplet and quintuplet excited states for each complex. A

broken symmetry approach was used in this study to permit electrons to be localized on different areas of the molecule, *i.e*., metal versus ligand, so they can couple magnetically but are not forcibly paired. The computed UV/Vis spectra were convoluted with Gaussian functions (FWMH = 1000 cm^{-1}), using GaussView software.

4. Results and Discussion

4.1. Elucidating the structural features of Cr-*p*H crucial to the Cr−to−L electron transfer

In order to elucidate the structural and electronic features that are crucial to give rise to the Cr−to−L electron transfer in **Cr-*p*H**, we performed a detailed broken symmetry DFT study. This approach allows to identify plausible structural motifs in trial structures or, at the opposite, to modify or reject trial structures containing incorrect motifs. At first, we verified that the chosen computational protocol was able to reproduce the geometrical experimental data. In the absence of structural data for **Cr-*p*H**, we considered the complex **$CrCl_3$OH-*p*H**, as sibling of **Cr-*p*H**, whose crystal structure was previously resolved.[38] In agreement with the experimental results,[38] in the most stable **$CrCl_3$OH-*p*H** structure Cr is octahedrally coordinated, with the ImPy ligand chelating to the metal and the OH group binding *trans* to the nitrogen atom of the pyridine moiety. A comparison between the most stable calculated geometry and the experimental X-ray structure reveals that all the key bond lengths differ less than 0.05 Å and the key angles no more than 2 deg (Table S1), confirming that the computational method chosen is able to lead to the correct geometrical features of the metal complexes investigated in this work. Afterwards, the **$CrCl_3$THF-*p*H** complex was optimized by DFT and a TDDFT analysis was performed to compare the computed UV−Vis spectrum with that recorded experimentally (Figure S1). In agreement with the corresponding experimental spectrum,[38] the most intense bands are observed in the 25000−28000 cm^{-1} range and only very weak bands appear in the region around 20000 cm^{-1}. These results confirm that the chosen computational method accurately reproduces the geometrical and electronic features of these chromium compounds.

Being confident of the chosen level of theory, we moved to consider the target complex **Cr-*p*H**. As abovementioned, no experimental structural data are available for **Cr-*p*H** and the elemental analysis are poorly informative. In contrast, the positive ion electrospray ionization mass spectra (ESI-MS) of **Cr-*p*H** shows two major ions at *m*/*z* 303 and 486, corresponding to $[LCrCl_2]^+$ and $[L_2CrCl_2]^+$ singly charged cations, respectively, and two minor peaks at *m*/*z* 344 and 386, corresponding to the acetonitrile adducts $[LCrCl_2{\cdot}CH_3CN]^+$ and $[LCrCl_2{\cdot}2CH_3CN]^+$, respectively (Figure S2). The ESI-MS study provides insights into the speciation of **Cr-*p*H** in solution, revealing the presence of multiple species and various coordinated entities, at least mono- and bis-ligated chromium compounds (Scheme 2). Unfortunately, considering the ESI-MS data as the sole source of

evidence cannot, in this case, provide unequivocal proof of the key conditions for the electron transfer to occur nor demonstrate the existence of specific isomers in solution. Indeed, due to the variety of coordination modes and potential dynamic process in solution, an unambiguous structural assignment of **Cr-*p*H** is not feasible.

We then proceeded modeling a wide range of geometries and spin states, starting from the experimental data in our hands. We focused on mono-ligated species of the type $LCrCl_2(THF)_n$ with different numbers of THF molecules coordinated to the metal and on bis-ligated complexes of the type L_2CrCl_2, whose presence is revealed by ESI-MS (Scheme 2). A total of four diverse structures were considered where mono-ligated and bis-ligated species are labeled with **M** and **B**, respectively, followed by a number which indicates the number of THF molecules in the complex **M**. For all of them, a charge 0 and a spin state of both 1 (triplet state) and 2 (quintet state) were systematically computed, and the ground state *S* value of these species was determined. The structural parameters and the spin state for the four complexes in their ground state are summarized in Figure 1.

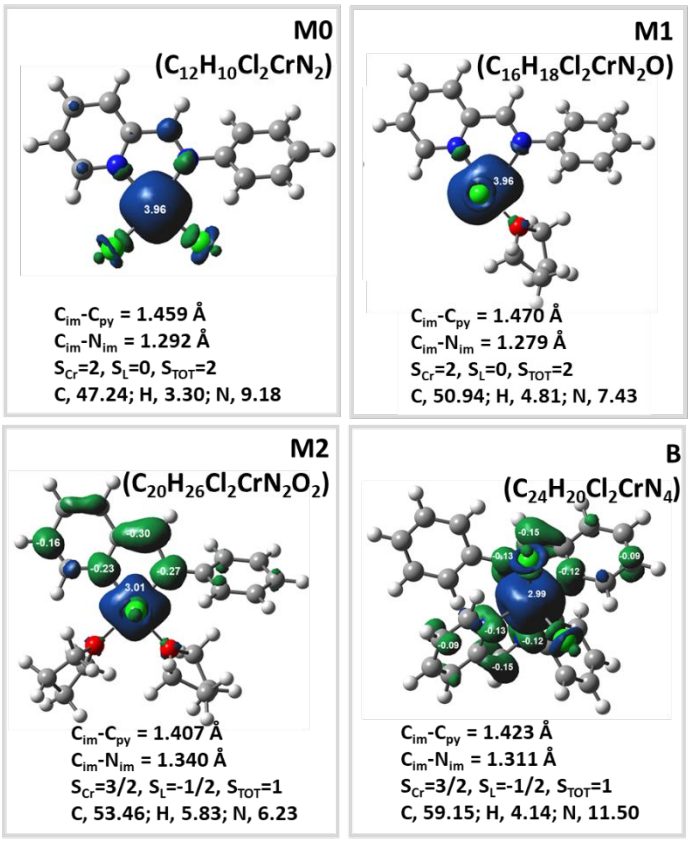

Figure 1. Mulliken spin densities (au, surfaces with 0.003 isovalue), main structural parameters, spin state and theoretical elemental analysis (C, H, N) data, for the four complexes computationally investigated in this work in their ground state. Positive spin density in blue and negative spin density in green.

Starting from the mono-ligated species, the number of THF molecules coordinated to Cr is crucial in affecting the ground electronic state and the occurrence of the electron transfer from Cr to

the ImPy ligand. In details, the naked Cr complex **M0** is more stable in the quintet state than in the triplet one by more than 20 kcal mol^{-1}, while for **M1** (with one THF co-ligand) the quintet state is calculated to be around 8 kcal mol^{-1} more stable than the triplet one. In both cases, the backbone C_{im}–C_{py} and the C_{im}–N_{im} bond lengths are those typical of the ligand in its neutral form (Scheme 1),[22] indicating the absence of the electron transfer. Accordingly, the spin density value on the metal center was calculated to be 3.96 in both cases, indicating the presence of four unpaired electrons on the Cr, *i.e.,* a *real* oxidation state of +2. The coordination of two molecules of THF in **M2**, instead, leads to the reduction of the ligand in both spin states with the most stable isomers showing a pretty similar octahedral coordination geometry. Only the isomer with two THF lying on the ligand plane and two Cl in the apical positions is discussed for brevity, the other structures calculated are reported in Table S2. In this case the ground state is the triplet one with the backbone C_{im}–C_{py} bond length of 1.407 Å and the C_{im}–N_{im} bond length of 1.340 Å. This relatively short C_{im}–C_{py} bond and long imine C_{im}–N_{im} bond are consistent with a singly reduced radical ligand $(L^{\bullet})^{-}$ (Scheme 1).[54] Accordingly, the computed spin density values were +3.01 on Cr, and −0.99 on the ligand (mainly on the pyridine moiety and C_{im}–N_{im} fragment), which indicates three unpaired electrons on Cr, antiferromagnetically coupled with the fourth electron transferred to the ligand. Hence, the *real* oxidation state of the Cr center is +3.

Moving to the bis-ligated species L_2CrCl_2, five different isomers can be identified (Chart 2). Among them, the performed energy calculations indicated **B*cis*-1** and **B*cis*-2** as isoenergetic and **B*cis*-3** only 1.7 kcal mol^{-1} higher in energy, thus an equilibrium between the different species can likely occur based on the thermodynamic data. On the contrary, the **B*trans*-1** and **B*trans*-2** isomers can be ruled out because the steric interactions between the two ligands cause a raise in energy to 8.0 and 4.8 kcal mol^{-1}, respectively. In any case, the bis-ligated species in the triplet state result to be more stable than the quintet ones. The computed structural parameters for all isomers are the same for the two ligands and intermediate between those characteristics of neutral and singly reduced radical ligands $(L^{\bullet})^{-}$. This is confirmed by the spin density map reported in Figure 1 for **B*cis*-1** as example, which indicates that a certain electron transfer occurs from Cr to the two ligands, resulting in three unpaired electrons on the Cr atom and around -0.5 spin density on each ligand.

Successively, for all the computed **Cr-*p*H** structures, we performed a computational UV−Vis analysis, and the simulated spectra were compared to the experimental ones in the attempt to identify the most probable population of the species in solution. Indeed, UV−Vis−NIR spectroscopy demonstrated to be a very sensitive tool for discriminating between neutral and charged redox ligands, the latter being characterized by very intense electronic transitions in the visible range.[38] For clarity, we report in Figure 2 only the simulated UV−Vis spectra of the most stable complexes discussed

above in their ground state (the three mono-ligated complexes, and the three more stable **B*cis*** isomers of the bis-ligated complex), compared to the experimental spectrum of **Cr-*p*H**. As already discussed in our previous work,[38] the UV−Vis−NIR spectrum of **Cr-*p*H** is characterized by intense (ε ≈ 3000−5000 $M^{-1}cm^{-1}$) absorption bands with a fine structure in the 21000–4000 cm^{-1} region (maxima observed at about 20000, 16500, 14000, 10500 and 5050 cm^{-1}), which have been generically assigned to intra-ligand π–π* transitions in π–radical monoanionic ligands of the type $(L^{\bullet})^{-}$. Similar intense bands have been reported for organometallic complexes bearing redox−active non−innocent ligands such as bpy or tpy, where an electron transfer occurs from the metal to the ligand, which is reduced to $(bpy^{\bullet})^{-}$ or $(tpy^{\bullet})^{-}$ (bpy = bipyridine, tpy = terpyridine).[55−57]

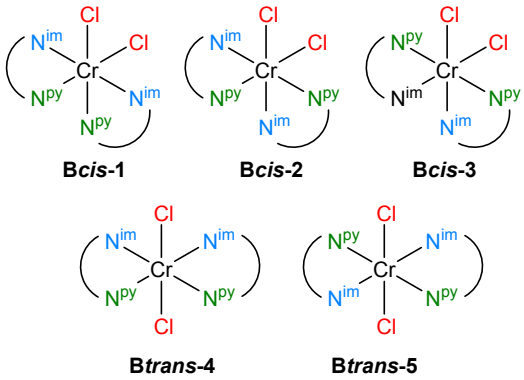

Chart 2. Sketches of the bis-ligated (B) isomers computationally investigated in this work.

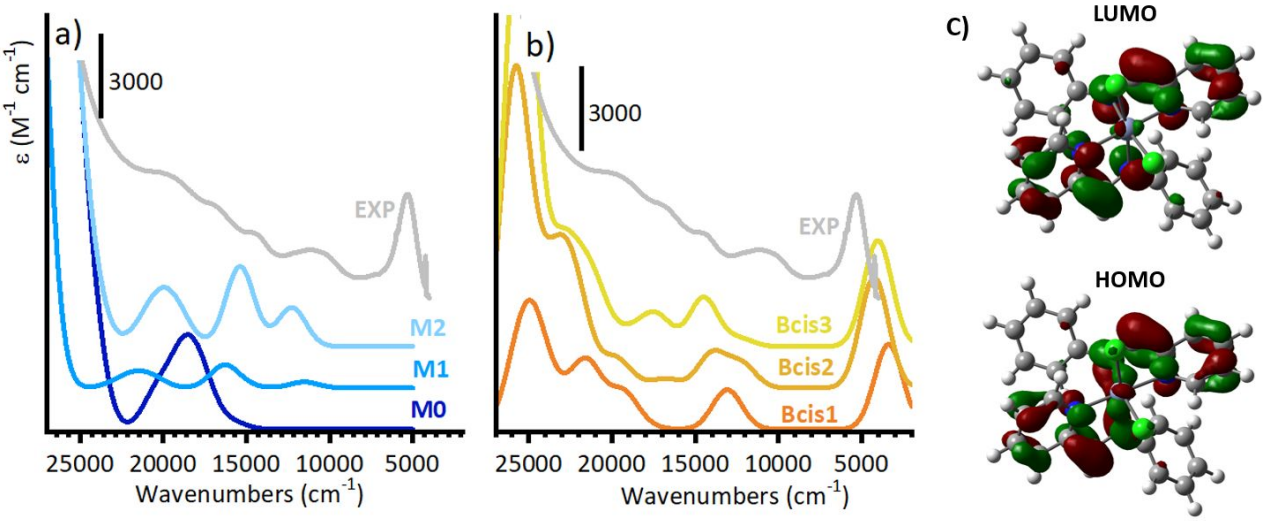

Figure 2. Simulated UV−Vis spectra some of the investigated complexes in their ground state, compared to the experimental UV−Vis−NIR spectrum of **Cr-*p*H** (EXP, after subtraction of the contribution of the solvent, CH_3Cl). Part a) refers to mono-ligated complexes, with either 0, 1 or 2 THF ligands; part b) refers to the three more stable *cis* isomers of the bis-legated complex. The spectra are vertically shifted for clarity. c) Molecular orbitals involved in the low energy transition at around 5000 cm^{-1} (β-HOMO → β-LUMO).

The simulated UV−Vis spectra for **M0** and **M1** (Figure 2a) do not reproduce the experimental spectrum at all. On the contrary, the simulated spectrum of **M2** shows bands of good intensity (ε ≈ 3000 $M^{-1}cm^{-1}$) in the region below 25000 cm^{-1}, with maxima at ≈20000, 15000 and 12000 cm^{-1}, even though it does not reproduce the experimentally observed band at about 5000 cm^{-1}. Analysis of the predicted bands in terms of the involved molecular orbitals allows for the assignment of the two transitions at lower frequencies (≈15000 and 12000 cm^{-1}) as ligand to metal charge transfer bands (LMCT). In both cases electron density is transferred from the radical ligand, in particular from pyridine and C_{im}–N_{im} fragment, to the Cr^{III} ion. Instead, the higher energy transition (≈ 20000 cm^{-1}) is predicted to be a ligand to ligand charge transfer band (LLCT), with the electron density transferred from the Cl ligand to the C_{py}–N_{py} and C_{im}–N_{im} orbitals of the ImPy ligand.

As for the bis-ligated complexes, the simulated UV−Vis−NIR spectrum (Figure 2b and Figure S3) displays a series of bands of medium intensity in the 21000–10000 cm^{-1} region which are due to LMCT transitions involving the pyridine and the C_{im}−N_{im} fragment. Clearly, the exact position of the bands varies according to the isomer structure. However, the distinctive feature of the simulated spectrum is a band centered around 5000 cm^{-1}, as intense as 3000−4000 M^{-1} cm^{-1}. Bands of equal intensity and similar position were previously reported for ligand mixed-valent species, *i.e.* bis- or tris-ligated complexes characterized by two or three equal ligands in a different redox state and ascribed to ligand−to−ligand intervalence charge-transfer transitions.[55,57,58] In our system, this band originates from a MLCT transition involving the HOMO orbital mainly centered on Cr and C_{im}, C_{py}, N_{im}, N_{py} atoms and the LUMO orbital delocalized on both ligands (Figure 2c). The participation of two ligands causes a meaningful stabilization of the LUMO orbital, decreasing sizably the HOMO−LUMO energy gap and the energy required for the transition. The analogue transition for **M2** occurs at around 12000 cm^{-1}.

Finally, inspired by the work recently reported in the literature,[59] we modeled an additional structure, consisting in a cationic bis-ligated Cr complex with a single Cl ligand, *i.e.*, $[L_2CrCl]^+$. The structure of the cationic bis-ligated $[L_2CrCl]^+$ is reported in Figure S4, with the relative spin density map and the simulated UV−Vis spectrum. Also the simulated UV−Vis−NIR spectrum of this complex is compatible with the experimental UV−Vis−NIR spectrum of **Cr-*p*H**, so the presence of this species cannot be excluded.

Overall, the computational analysis summarized above clearly indicates that the Cr−to−L electron transfer is promoted either by the presence of two THF co-ligands in the coordination sphere of the metal in a mono-ligated form, or by the formation of a bis-ligated species. Comparison between simulated and experimental UV−Vis−NIR spectra suggests that several chromium species might

coexist in **Cr-*p*H**, comprising mono-ligated species with two THF coordinated, and both neutral and cationic bis-ligated species, in good agreement with the ESI-MS results.

4.2. *Para*-Aryl Substituted Chromium Complexes

After having identified the features responsible for the occurrence of the Cr−to−L electron transfer in **Cr-*p*H**, we proceeded to systematically modify the electron donor strength of the ImPy ligand. This was achieved by introducing different substituents at the 4-position of the aryl moiety (namely, OCH_3, CH_3, CF_3 see Chart 1), which are expected to have an electronic rather than a steric effect, being the chromium centre in a distal position. In the absence of structural data in hand, and in view of the paramagnetism of the complexes (which makes ^{1}H NMR poorly informative), we turned again our attention to optical spectroscopies (IR and UV−Vis−NIR).

Figure 3 shows the ATR-IR spectra of all the ligands (part a) and Cr complexes (part b) investigated in this work in the most significant frequency range. Generally speaking, the absorption bands around 1625 cm^{-1} observed in the spectra of the ligands (Figure 3a) are ascribed to the almost pure ν(C=N) vibration of the imine group. The bands observed in the 1600–1000 cm^{-1} range are mainly due to in-plane δ(C-H) vibrations involving either the pyridine or the aryl moiety or the whole skeleton, while below 1000 cm^{-1} most of the bands are due to out-of-plane δ(C-H) modes. The spectra of the *para*-aryl substituted ligands are pretty similar to that of **L*p*H**, except for the presence of a few additional intense absorption bands prevalently due to in-plane δ(C-H) vibrational modes of the *para*-aryl substituted moiety involving substantial changes of the C(aryl)–substituent bond length and/or angle. For example, **L*p*OCH$_3$** shows intense bands at about 1505 and 1240 cm^{-1}, which are associated to vibrational modes involving the stretching of the C–(OCH_3) bond. **L*p*CF$_3$** shows intense bands at about 1320 and 1106 cm^{-1}, ascribed to collective vibrations involving the stretching of the C–(CF_3) bond.

As already reported for **Cr-*p*H**,[38] the ATR-IR spectra of the Cr complexes (Figure 3b) are sensibly different from those of the corresponding ligands. In all the cases, the sharp band characteristic for the ν(C=N) vibration of the imine group around 1625 cm^{-1} shifts and the group of narrow bands in the 1650−1400 cm^{-1} is substituted by a more intense and broad band centred around 1600 cm^{-1} as a consequence of ligand complexation. In the 1400–1000 cm^{-1} region the spectra of the complexes are much simpler than those of the corresponding ligands, with apparently fewer bands, enhanced in intensity and broadened. A broadening and intensification of several specific skeletal vibrational modes, which are efficiently coupled to electronic transition and hence generate large molecular dipole changes, is well documented for radical anions of conjugated molecules.[60,61] Hence,

the ATR-IR spectra reported in Figure 3b suggest that in all the complexes the ligand **L*p*R** is not neutral, but rather in its (**L*p*R•**)$^{-}$ π-radical anionic form, as already demonstrated for **Cr-*p*H**.[38]

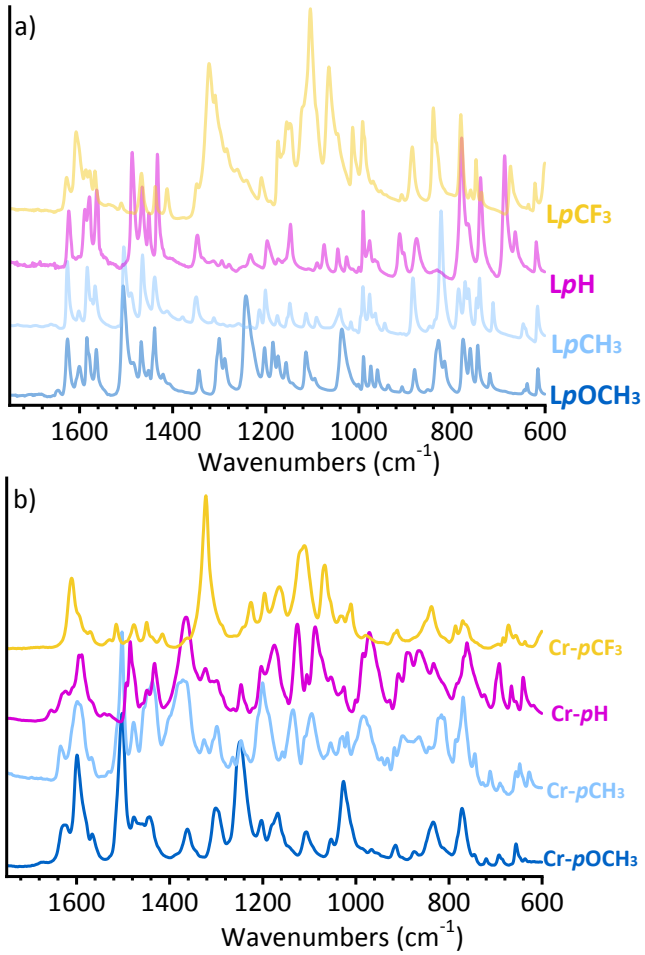

Figure 3. ATR-IR spectra of the ligands (part a) and the corresponding chromium complexes (part b). The spectra are vertically stacked for clarity.

A confirmation of the radical anionic nature of the ligand in the investigated complexes comes from UV−Vis−NIR spectroscopy. Due to the poor solubility of some of the complexes, we measured the spectra in reflectance mode on samples in the solid state, which are shown in Figure 4a. Notably, the DR UV−Vis−NIR spectrum of **Cr-*p*H** is identical to that collected in transmission mode on a chloroform solution, indicating that a complex mixture of different Cr species exists also in the solid state and that the main species are the same as those observed in solution. The UV−Vis−NIR spectra of **Cr-*p*OCH$_3$** and **Cr-*p*CH$_3$** are very much similar to that of **Cr-*p*H,** strongly suggesting that they also present a Cr formally in its oxidized state +3, antiferromagnetically coupled to the ligand(s) in the reduced state (**L*p*R•**)$^{-}$. In contrast, the spectrum of **Cr-*p*CF$_3$** is pretty different because it shows an intense and broad absorption centred at about 16000 cm^{-1}, but no bands at lower frequency.

At this point we moved to computationally investigate the effect of the different substitution at the *N*−aryl *para* position on the electronic properties of the complexes. In the absence of structural

experimental data, we computed all the synthesized complexes taking into account both the mono-ligated species with two THF molecules coordinated to Cr (**M2−*p*R**) and the bis-ligated species (**B**), in agreement with ESI-MS data. The calculated geometries indicate that the **M2−*p*R** complexes in the triplet ground state show a reduced ligand. Similarly, in the **B−*p*R** complexes in the quintet state, a certain electron transfer occurs from Cr to the two ligands.

The simulated UV−Vis spectra (Figure 4b and 4c) seem poorly affected by the ligand substituents. In particular, the simulated UV−Vis spectra of **M2-*p*CH$_3$** and **M2-*p*OCH$_3$** are identical to that of unsubstituted **M2-*p*H**, in agreement with the experimental observation. The only exception is that of **M2-*p*CF3**, which shows an intense band at ~18000 cm^{-1}, much less visible in the simulated spectra of the other mono-ligated complexes.

As far as the bis-ligated species is concerned, the simulated UV−Vis spectra of all the complexes are almost identical below 16000 cm^{-1}, while they mainly differ for the position of the LLCT band at around 21000 cm^{-1}.

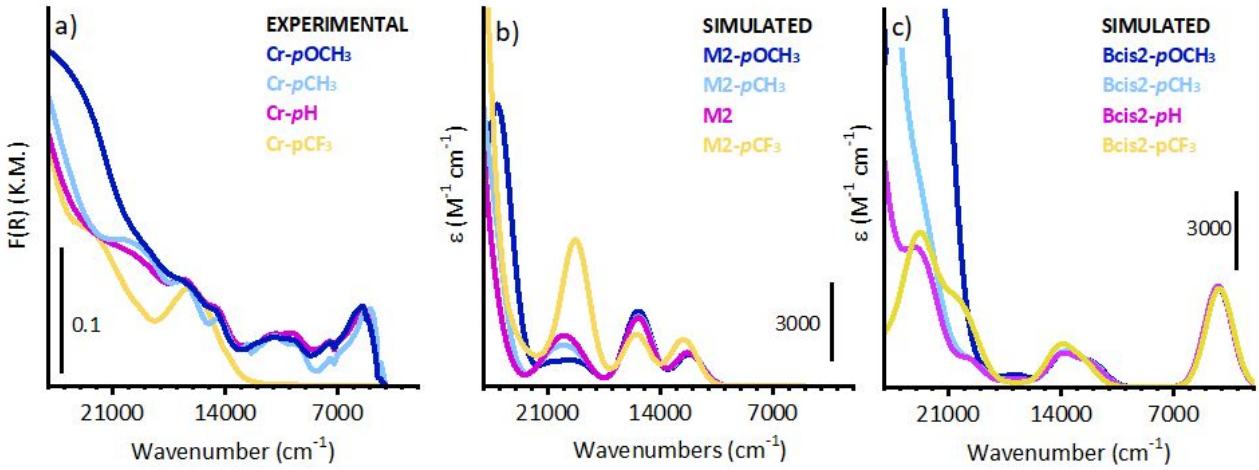

Figure 4. DR UV−Vis spectra of the chromium complexes synthetized in this work (part a) compared to the simulated UV−Vis spectra for the **M2-*p*R** (part b) and **Bcis2-*p*R** (part c) complexes in their ground state.

The spectra suggest that **Cr-*p*OCH$_3$** and **Cr-*p*CH$_3$** have electronic features pretty much similar one to each other and to **Cr-*p*H**, hence they are dominated by bis-ligated species, which account for the intense band at 5000 cm^{-1}, even though the presence of **M2** species cannot be discarded. In contrast, **Cr-*p*CF$_3$** prefers to remain in the mono-ligated form with Cr coordinated to two THF. In all cases a Cr−to−L electron transfer occurs.

4.3. Polymerization of Ethylene

Combining the findings from our current study with previous data,[38] we observe a significant influence of the *N*−aryl substituents' position (*ortho* vs *para*) on the formation of the reduced π radical

ImPy anion, as supported by both calculations and UV−VIS measurements. In the following, we demonstrate that the preliminary data concerning the reactivity of the investigated precatalysts in the ethylene polymerization are fully consistent with the hypothesis first advanced by some of us,[38] that is that the concerted Cr−to−L electron transfer is essential in facilitating the polymerization of ethylene.

The catalytic utility of all the synthesized complexes was first evaluated in the polymerization of ethylene under a constant ethylene pressure (1 atm) using MAO as the alkylating reagent (250 equiv of Al to Cr). The catalytic tests were conducted at room temperature using a low chromium loading to easily maintain the temperature throughout the polymerization without cooling in the early stages. The polymerization reactions were stopped rapidly to avoid mass transport limitations caused by filling of the reactor with the swollen polymer and precipitation, which may have otherwise adversely impacted our preliminary data.[32] Polymerization conditions and results are summarized in Table 1.

Table 1. Results of ethylene polymerization experiments.[a]

entry	complex	T (°C)	PE (g)	activity[b]	M_w[c] (g mol^{-1})	M_w/M_n[c]	T_m[d] (°C)
1	**Cr-*p*CF$_3$**	20	0.51	3200	1.9×10^6	2.0	140
2	**Cr-*p*H**	20	0.29	1800	5.1×10^5	4.0	137
3	**Cr-*p*CH$_3$**	20	0.16	980	5.8×10^5	4.2	138
4[e]	**Cr-*p*OCH$_3$**	20	0.09	70	4.3×10^5	5.0	137
5	**Cr-*p*CF$_3$**	40	0.53	3300	1.2×10^6	2.8	138
6	**Cr-*p*CF$_3$**	60	0.50	3120	M_{p1}[f] $= 10\times10^3$ M_{p2}[g] $= 215\times10^3$		132

[a] Polymerization conditions: ethylene pressure, 1.01 bar; total volume, 25 mL (toluene); Cr-complex (2.4 μmol) solution in dry CH_2Cl_2; Al/Cr = 250; time, 4 min. [b] Activity in $kg_{PE}\ mol_{Cr}^{-1}h^{-1}$. [c] average molecular weight (M_w) and molecular weight distribution (M_w/M_n) determined by SEC. [d] Melting temperature (T_m) determined by DSC (second heating). [e] Cr, 10 μmol and polymerization time, 8 min. [f] M_{p1} is the peak molecular weight of the low−MW fraction (Figure S5). [g] M_{p2} is the peak molecular weight of the high−Mw fraction (Figure S5).

The electronic perturbation induced by substituents at the *N*−aryl *para* position brings a pronounced effect on the catalytic activity. The investigated Cr precatalysts exhibit from low to very high activity in the polymerization of ethylene. By far **Cr-*p*CF$_3$** exhibited the highest initial activity (Table 1, entry 1). The inclusion of an electron-withdrawing substituents onto the ImPy ligand skeleton generally increases the catalyst's activity in the order **Cr-*p*OCH$_3$** (70 kg(PE) mol(Cr)$^{-1}$ h^{-1}) < **Cr-*p*CH$_3$** (980) < **Cr-*p*H** (1800) < **Cr-*p*CF$_3$** (3200). The high activity of **Cr-*p*CF$_3$** may be related to the formation, in the presence of MAO, of a more easily accessible and even more electron-deficient coordination active sites, thereby promoting the chain propagation rate.[62−64] In contrast to the accelerating effect of the CF_3 substituent, the placement of stronger electron-donating methyl−

and methoxy−*para*-substituents has a negative effect on the activity. Considering the donor character of **L*p*CH$_3$** and **L*p*OCH$_3$**, a more strongly electron donating ligand may stabilize the catalytically active species, making the coordination of the incoming ethylene more difficult.[65] For **Cr-*p*OCH$_3$**, only very small amount of PE was isolated, and only very low ethylene consumption was detected within the first minutes.

The obtained PEs are solid, fully saturated, semicrystalline polymers with very high molecular weight ($M_w > 10^5$ g/mol), monomodal molecular weight distribution ($2.0 < M_w/M_n < 5.0$) and melting temperature (T_m) ranging from 137 to 140 °C. The placement of the CF_3 *para*−aryl substituent facilitate the formation of UHWMPE: M_w exceeds 10^6 g mol^{-1} while the molecular weight distribution remains quite narrow (M_w/M_n = 2.0 − Figure S5). Besides, in contrast to the decelerating effect of methyl− and methoxy− *para*-substituents on the polymerization rate, the substitution of an H at the *para*−aryl position by more electron-donating substituents has no negative effect on the molecular weight of the resultant polymers. The polymer molecular weight may hardly be correlated to the ligand electronic properties. Additional effects such as steric interaction of the ligand with the last inserted ethylene unit may complicate the recognition of clear trends.

The effect of polymerization temperature on the catalytic behavior was further studied with **Cr-*p*CF$_3$** (Table 1, entry 5 and 6). **Cr-*p*CF$_3$** exhibits an activity as high as 3300 kg(PE) mol(Cr)$^{-1}$ h^{-1} and affords a UHMWPE ($M_w = 1.2 \times 10^6$ g mol^{-1}) even at 40 °C, thereby demonstrating a good early thermal stability and high propensity to insert ethylene. Further increase of the polymerization temperature from 40 to 60 °C led only to smooth decrease in activity, while the SEC analysis of the resultant polymer shows a bimodal distribution which well correlates with a dominant chain transfer at higher temperature. The shape of the SEC curves of sample 6 is dominated by two components with a low−MW (M_{p1} in Table 2) and a high−MW (M_{p2}) (Figure S5). This data may be ascribed to the higher propensity at higher reaction temperature to undergo β−H elimination at a last enchained ethylene unit followed by chain termination prior to the subsequent and fast ethylene coordination and insertion. [66−69]

5. CONCLUSIONS

Due to their intricate structural chemistry and redox-active properties, ImPys have been the center of attention for years as ligands for several transition metals to be employed in different catalytic processes. Their application has recently broadened to include chromium and olefin polymerization. Despite the initial belief that ImPys possessed the ideal "structural" motif to generate complexes for the oligomerization of ethylene rather than its polymerization, we discovered that the simple unsubstituted aldimine when paired with *formally* divalent chromium, **Cr-*p*H,** efficiently polymerizes ethylene to give high−MW PEs.[38] We established that a concerted Cr−to−L electron transfer, which

transitions the ImPy ligand to its monoanionic radical $(L^{\bullet})^{-}$ state and the chromium to a trivalent *physical* oxidation state, is essential for facilitating the polymerization of ethylene.

However, so far the structural and electronic features crucial for the Cr−to−L electron transfer in **Cr-*p*H** were not clearly understood. In this work, we aimed to bridge this knowledge gap by synergistically combining UV−Vis−NIR spectroscopy with DFT calculations, thereby overcoming the lack of structural data. We demonstrated that the Cr−to−L electron transfer is either promoted in the presence of two THF co-ligands for mono-ligated complexes (*i.e.*, $LCrCl_2(THF)_2$), or by the formation of bis-ligated complexes of the type L_2CrCl_2. Experimental ESI-MS data and UV−Vis−NIR spectrum of **Cr-*p*H** suggest the co-existence of multiple species.

Subsequently, we expanded the library of ImPy−Cr complexes. Substituents (*i.e.*, CH_3, OCH_3 and CF_3) were appended at the *para*-aryl 4-position on the aniline moiety. UV−Vis−NIR and IR spectroscopy clearly demonstrate that **Cr-*p*CH$_3$** and **Cr-*p*OCH$_3$** share the same electronic properties as **Cr-*p*H**, involving a complex equilibrium between different species (mono- and bis-ligated chromium compounds). In contrast, **Cr-*p*CF$_3$** emerges as an exception, likely consisting mainly of mono-ligated species bearing two THF co-ligands in the chromium coordination sphere. The complexes exhibit a range of polymerization activity, from low to high, strongly influenced by the electron donating/withdrawing ability of the ligand substituent. Notably, UHMWPEs (MW > 10^6 g mol^{-1}) with monomodal and narrow molecular weight distribution are achievable with **Cr-*p*CF$_3$**/MAO even at 40 °C.

ACKNOWLEDGEMENTS

This work was supported by the project “Cr4FUN - Chromium catalysis: from fundamental understanding to functional aliphatic polymers” funded by MUR Progetti di Ricerca di Rilevante Interesse Nazionale (PRIN) Bando 2017 (20179FKR77_002). We are grateful to Fabio De Stefano and Daniele Piovani for DSC and SEC measurements, respectively, Anna Maria Fovanna, Rocco Di Girolamo and Benedetta Palucci for helpful discussion.

ASSOCIATED CONTENT

The Supporting Information is available free of charge on the ACS Publications website at DOI

- Computational details; Key structural parameters for the most stable calculated geometry for **CrCl$_3$OH-*p*H**; Computed and experimental UV−Vis−NIR spectrum for **CrCl$_3$THF-*p*H**; Simulated UV−Vis spectra of the five bis-ligated isomers having a **Cr-*p*H** structure; Mulliken spin densities, main structural parameters and spin state, and simulated UV−Vis−NIR spectrum for the cationic $[L_2CrCl]^+$ complex in its ground state; Cartesian coordinates of species discussed in the manuscript; SEC curve of PEs (PDF).

REFERENCES

[1] Nowlin, T.E. Business and Technology of the Global Polyethylene Industry, Wiley-Scrivener, New York, **2014**.

[2] McDaniel, M.P. A Review of the Phillips Supported Chromium Catalyst and Its Commercial Use for Ethylene Polymerization. *Adv. Catal*. **2010**, *53*, 123–606.

[3] Wang, X.Y.; Gao, Y.; Tang, Y. Sustainable developments in polyolefin chemistry: Progress, challenges, and outlook. *Prog. Polym. Sci*. **2023**, *143*, 101713.

[4] Capacchione, C.; Grisi, F.; Lamberti, M.; Mazzeo, M.; Milani, B.; Milione, S.; Pappalardo, D.; Zuccaccia, C.; Pellecchia, C. Metal Catalyzed Polymerization: From Stereoregular Poly(α-olefins) to Tailor-Made Biodegradable/Biorenewable Polymers and Copolymers. *Eur. J. Inorg. Chem*. **2023**, e202200644.

[5] Zhang, Y.; Zhang, Y.; Jian, Z. A comprehensive picture on chain walking olefin polymerization. *Polymer* **2023**, *265*, 125578.

[6] Balzade, Z.; Sharif, F.; Ghaffarian Anbaran, S. R. Tailor-Made Functional Polyolefins of Complex Architectures: Recent Advances, Applications, and Prospects. *Macromolecules* **2022**, *55*, 6938–6972.

[7] Dau, H.; Jones, G.R.; Tsogtgerel, E.; Nguyen, D.; Keyes, A.; Liu, Y.S.; Rauf, H.; Ordonez, E.; Puchelle, V.; Basbug Alhan, H.; Zhao, C.; Harth, E. Linear Block Copolymer Synthesis. *Chem. Rev.* **2022**, *122*, 14471–14553.

[8] Jasinska-Walc, L.; Bouyahyi, M.; Duchateau, R. Potential of Functionalized Polyolefins in a Sustainable Polymer Economy: Synthetic Strategies and Applications. *Acc. Chem. Res*. **2022**, *55*, 1985−1996.

[9] Tan, C.; Zou, C.; Chen, C. Material Properties of Functional Polyethylenes from Transition-Metal-Catalyzed Ethylene–Polar Monomer Copolymerization. *Macromolecules* **2022**, *55*, 1910–1922

[10] Zanchin, G.; Leone, G. Polyolefin thermoplastic elastomers from polymerization catalysis: Advantages, pitfalls and future challenges. *Prog. Polym. Sci.* **2021**, *113*, 101342.

[11] Wu, R.; Wu, W. K.; Stieglitz, L.; Gaan, S.; Rieger, B.; Heuberger, M. Recent advances on α-diimine Ni and Pd complexes for catalyzed ethylene (Co)polymerization: A comprehensive review. *Coord. Chem. Rev.* **2023**, *474*, 214844.

[12] Phillips, A.M.F.; Suo, H.; Guedes da Silva, M.C.; Pombeiro, A. J. L.; Sun, W.H. Recent developments in vanadium-catalyzed olefin coordination polymerization. *Coord. Chem. Rev*. **2020**, *416*, 213332.

[13] Yuan, S.F.; Yan, Y.; Solan, G.A.; Ma, Y.; Sun, W.H. Recent advancements in N-ligated group 4 molecular catalysts for the (co)polymerization of ethylene. *Coord. Chem. Rev.* **2020**, *411*, 213254.

[14] Champouret, Y.; Hashmi, O. H.; Visseaux, M. Discrete iron-based complexes: Applications in homogeneous coordination-insertion polymerization catalysis. *Coord. Chem. Rev.* **2019**, *390*, 127–170.

[15] Xing, Y.; Wang, L.; Yu, H.; Khan, A.; Haq, F.; Zhu, L. Recent progress in preparation of branched polyethylene with nickel, titanium, vanadium and chromium catalytic systems and EPR study of related catalytic systems. *Eur. Poly. J.* **2019**, 109339.

[16] Stürzel, M.; Mihan, S.; Mülhaupt, R. From Multisite Polymerization Catalysis to Sustainable Materials and All-Polyolefin Composites. *Chem. Rev.* **2016**, *116*, 1398–1433.

[17] Kaim, W. Manifestations of noninnocent ligand behavior. *Inorg. Chem*. **2011**, *50*, 9752−65.

[18] Praneeth, V. K.; Ringenberg, M. R.; Ward, T. R. Redox-active ligands in catalysis. *Angew. Chem., Int. Ed.* **2012**, *51*, 10228−34.

[19] Luca, O. R.; Crabtree, R. H. Redox-active ligands in catalysis. *Chem. Soc. Rev*. **2013**, *42*, 1440−59.

[20] van der Vlugt, J. I. Radical-Type Reactivity and Catalysis by Single-Electron Transfer to or from Redox-Active Ligands. *Chem.-Eur. J.* **2019**, *25*, 2651−2662.

[21] Arevalo, R.; Chirik, P. J. Enabling Two-Electron Pathways with Iron and Cobalt: From Ligand Design to Catalytic Applications. *J. Am. Chem. Soc.* **2019**, *141*, 9106−9123.

[22] Lu, C. C.; Bill, E.; Weyhermüller, T.; Bothe, E.; Wieghardt, K. Neutral Bis(α-Iminopyridine)Metal Complexes of the First-Row Transition Ions (Cr, Mn, Fe, Co, Ni, Zn) and Their Monocationic Analogues: Mixed Valency Involving a Redox Noninnocent Ligand System. *J. Am. Chem. Soc.* **2008**, *130*, 3181–3197.

[23] Ge, Y.; Lu, Z.; Dai, S. Flexible Axial Shielding Strategy for the Synthesis of High-Molecular-Weight Polyethylene and Polar Functionalized Polyethylene with Pyridine-Imine Ni(II) and Pd(II) Complexes. *Organometallics* **2022**, *41*, 2042–2049.

[24] Wang, C.; Zhang, Y.; Mu, H.; Jian, Z. Systematic Studies on Dibenzhydryl and Pentiptycenyl Substituted Pyridine-Imine Nickel(II) Mediated Ethylene Polymerization. *Dalton Trans.* **2020**, *49*, 4824–4833.

[25] Chen, Z.; Allen, K. E.; White, P. S.; Daugulis, O.; Brookhart, M. Synthesis of Branched Polyethylene with "Half-Sandwich" Pyridine-Imine Nickel Complexes. *Organometallics* **2016**, *35*, 1756–1760.

[26] Chen, X. L.; Gao, J.; Liao, H.; Gao, H. Y.; Wu, Q. Synthesis, Characterization, and Catalytic Ethylene Oligomerization of Pyridine-Imine Palladium Complexes. *Chin. J. Chem. Eng*. **2018**, *36*, 176–184.

[27] Yan, Z.; Bi, H.; Ding, B.; Wang, H.; Xu, G.; Dai, S. A Rigid-Flexible Double-Layer Steric Strategy for Ethylene (Co)Oligomerization with Pyridine-Imine Ni(II) and Pd(II) Complexes. *New J. Chem.* **2022**, *46*, 8669–8678.

[28] Chen, A.; Liao, D.; Chen, C. Promoting Ethylene (Co)Polymerization in Aliphatic Hydrocarbon Solvents Using Tert-Butyl Substituted Nickel Catalysts. *Chin. J. Chem.* **2022**, *40*, 215–222.

[29] Dall'Anese, A.; Fiorindo, M.; Olivieri, D.; Carfagna, C.; Balducci, G.; Alessio, E.; Durand, J.; Milani, B. Pd-Catalyzed CO/Vinyl Arene Copolymerization: When the Stereochemistry Is Controlled by the Comonomer. *Macromolecules* **2020**, *53*, 7783–7794.

[30] Rosar, V.; Dedeic, D.; Nobile, T.; Fini, F.; Balducci, G.; Alessio, E.; Carfagna, C.; Milani, B. Palladium Complexes with Simple Iminopyridines as Catalysts for Polyketone Synthesis. *Dalton Trans*. **2016**, *45*, 14609–14619.

[31] Rapallo, A.; Porzio, W.; Zanchin, G.; Ricci, G.; Leone, G. 2,3-*exo*-Diheterotactic Dicyclopentadiene Oligomers: An X-ray Powder Diffraction Study of a Challenging Multiphase Case. *Chem. Mater*. **2019**, *31*, 6650−6664.

[32] Leone, G.; Salamone, A.; Palucci, B.; Zanchin, G.; Groppo, E.; Forni, A. High−molecular weight poly(2-substituted 1,3-diene)s using iminopyridine iron precatalysts at high polymerization temperature and low iron loading. *Polymer* **2023**, 288, 126452.

[33] Yuan, R.; Ren, G.; Mahmood, Q.; Zeng, Y.; Wang, Y.; Liang, T.; Sun, W.H. Cycloheptyl-Fused Iminopyridine-Iron Catalysts for Isoprene Polymerization with Enhanced Activity and Thermal Stability. *Organometallics* **2023**, *42*, 3307−3318

[34] Ricci, G.; Leone, G.; Zanchin, G.; Palucci, B.; Boccia, A.C.; Sommazzi, A.; Masi, F.; Zacchini, S.; Guelfi, M.; Pampaloni, G. Highly stereoregular 1,3-butadiene and isoprene polymers through monoalkyl-N-Aryl-Substituted iminopyridine iron complex-based catalysts: synthesis and characterization. *Macromolecules* **2021**, *54*, 9947–9959.

[35] Hashmi, O.H.; Champouret, Y.; Visseaux, M. Highly active iminopyridyl iron-based catalysts for the polymerization of isoprene. *Molecules* **2019**, *24*, 3024.

[36] Guo, L.; Jing, X.; Xiong, S.; Liu, W.; Liu, Y.; Liu, Z.; Chen, C. Influences of alkyl and aryl substituents on iminopyridine Fe(II)- and Co(II)-Catalyzed isoprene polymerization. *Polymers* **2016**, *8*, 389.

[37] Zanchin, G.; Piovano, A.; Amodio, A.; De Stefano, F.; Di Girolamo, R.; Groppo, E.; Leone, G. NEt_3-Triggered Synthesis of UHMWPE Using Chromium Complexes Bearing Non-innocent Iminopyridine Ligands. *Macromolecules* **2021**, *54*, 1243−1253.

[38] Leone, G.; Groppo, E.; Zanchin, G.; Martino, G. A.; Piovano, A.; Bertini, F.; Martí-Rujas, J.; Parisini, E.; Ricci, G. Concerted Electron Transfer in Iminopyridine Chromium Complexes: Ligand Effects on the Polymerization of Various (Di)olefins. *Organometallics* **2018**, *37*, 4827−4840.

[39] Lu, C.C.; DeBeer George, S.; Weyhermüller, T.; Bill, E.; Bothe, E.; Wieghardt. K. An Electron-Transfer Series of High-Valent Chromium Complexes with Redox Non-Innocent, Non-Heme Ligands. *Angew. Chem. Int. Ed.* **2008**, *47*, 6384 –6387.

[40] McDaniel, A. M.; Rappé, A. K.; Shores, M.P. Structural and Electronic Comparison of 1st Row Transition Metal Complexes of a Tripodal Iminopyridine Ligand. *Inorg. Chem*. **2012**, *51*, 12493−12502.

[41] McDaniel, A. M.; Tseng, H.W.; Hill, E. A.; Damrauer, N. H.; Rappé, A. K.; Shores, M. P. Syntheses and Photophysical Investigations of Cr(III) Hexadentate Iminopyridine Complexes and Their Tris(Bidentate) Analogues. *Inorg. Chem.* **2013**, *52*, 1368−1378.

[42] McGuinness, D. S. Olefin Oligomerization via Metallacycles: Dimerization, Trimerization, Tetramerization, and Beyond. *Chem. Rev*. **2011**, *111*, 2321−2341.

[43] Diez, V.; Cuevas, J. V.; García-Herbosa, G.; Aullón, G.; Charmant, J. P.; Carbayo, A.; Munoz, A. ^{1}H NMR Direct Observation of Enantiomeric Exchange in Palladium (II) and Platinum (II) Complexes Containing N,N‘ Bidentate Aryl-pyridin-2-ylmethyl-amine Ligands. *Inorg. Chem*. **2007**, *46*, 568−577.

[44] Dong, Y. W.; Fan, R. Q.; Wang, X. M.; Wang, P.; Zhang, H. J.; Wei, L. G.; Chen, W.; Yang, Y. L. (*E*)-N-(Pyridine-2-ylmethylene) arylamine as an Assembling Ligand for Zn (II)/Cd (II) Complexes: Aryl Substitution and Anion Effects on the Dimensionality and Luminescence Properties of the Supramolecular Metal–Organic Frameworks. *Cryst. Growth Des.* **2016,** *16*, 3366−3378.

[45] Harding, P.; Harding, D. J.; Soponrat, N.; Tinpun, K.; Samuadnuan, S.; Adams, H. Synthesis and Electrochemical Studies of Nickel β-Diketonate Complexes Incorporating Asymmetric Diimine Ligands. *Aust. J. Chem.* **2010**, *63*, 75−82.

[46] (a) Small, B. L.; Carney, M. J.; Holman, D. M.; O’Rourke, C. E.; Halfen, J. A. New Chromium Complexes for Ethylene Oligomerization: Extended Use of Tridentate Ligands in Metal-Catalyzed Olefin Polymerization. *Macromolecules* **2004**, *37*, 4375−4386. (b) Kreisel, K.A.; Yap, G.P.A.; Theopold, K. H. Synthesis, Characterization, and Electronic Structure of Diimine Complexes of Chromium. *Inorg. Chem*. **2008**, *47*, 5293−5303.

[47] Frisch, M. J.; Trucks, G. W.; Schlegel, H. B.; Scuseria, G. E.; Robb, M. A.; Cheeseman, J. R.; Montgomery, J. A.; Vreven, T.; Kudin, K. N.; Burant, J. C.; Millam, J. M.; Iyengar, S. S.; Tomasi, J.; Barone, V.; Mennucci, B.; Cossi, M.; Scalmani, G.; Rega, N.; Petersson, G. A.; Nakatsuji, H.; Hada, M.; Ehara, M.; Toyota, K.; Fukuda, R.; Hasegawa, J.; Ishida, M.; Nakajima, T.; Honda, Y.;

Kitao, O.; Nakai, H.; Klene, M.; Li, X.; Knox, J. E.; Hratchain, H. P.; Cross, J. B.; Adamo, C.; Jaramillo, J.; Gomperts, R.; Stratmann, R. E.; Yazyev, O.; Austin, A. J.; Cammi, R.; Pomelli, C.; Ochterski, J. W.; Ayala, P. Y.; Morokuma, K.; Voth, G. A.; Salvador, P.; Dannenberg, J. J.; Zakrzewski, V. G.; Dapprich, S.; Daniels, A. D.; Strain, M. C.; Farkas, O.; Malick, D. K.; Rabuck, A. D.; Raghavachari, K.; Foresman, J. B.; Ortiz, J. V.; Cui, Q.; Baboul, A. G.; Clifford, S.; Cioslowski, J.; Stefanov, B. B.; Liu, G.; Liashenko, A.; Piskorz, P.; Komaromi, I.; Martin, R. L.; Fox, D. J.; Keith, T.; Al-Laham, M. A.; Peng, C. Y.; Nanayakkara, A.; Challacombe, M.; Gill, P. M. W.; Johnson, B.; Chen, W.; Wong, M. W.; Gonzalez, C.; Pople, J. A. B.1 ed., Gaussian, Inc., Pittsburgh PA, **2009**.

[48] Lee, C.; Yang, W.; Parr, R. G. Development of the Colle-Salvetti correlation-energy formula into a functional of the electron density. *Phys. Rev. B* **1998**, *37*, 785−789.

[49] Becke, A. D. Density-functional exchange-energy approximation with correct asymptotic behavior. *Phys. Rev. A* **1988**, *38*, 3098−3100.

[50] Becke, A. D. Density-functional thermochemistry. III. The role of exact exchange. J. *Chem. Phys.* **1993**, *98*, 5648−5652.

[51] Weigend, F.; Ahlrichs, R. Balanced basis sets of split valence, triple zeta valence and quadruple zeta valence quality for H to Rn: Design and assessment of accuracy. *Phys. Chem. Chem. Phys.* **2005**, *7*, 3297−3305.

[52] Haeusermann, U.; Dolg, M.; Stoll, H.; Preuss, H. Accuracy of energy-adjusted quasi-relativistic ab initio pseudopotentials - all-electron and pseudopotential benchmark calculations for HG, HGH and their cations. *Mol. Phys*. **1993**, *178*, 1211−1224.

[53] Kuechle, W.; Dolg, M.; Stoll, H.; Preuss, H. Energy-adjusted pseudopotentials for the actinides - parameter sets and test calculations for thorium and thorium monoxide. *J. Chem. Phys*. **1994**, *100*, 7535−7542.

[54] Zhou, W.; Chiang, L.; Patrich, B. O.; Storr, T.; Smith, K. M. Cyclopentadienyl chromium diimine and pyridine-imine complexes: ligand-based radicals and metal-based redox chemistry. *Dalton Trans*. **2012**, *41*, 7920−7930.

[55] Scarborough, C. C.; Lancaster, K. M.; DeBeer, S.; Weyhermüller, T.; Sproules, S.; Wieghardt, K. Experimental Fingerprints for Redox-Active Terpyridine in $[Cr(tpy)_2](PF_6)_n$ (n = 3–0), and the Remarkable Electronic Structure of $[Cr(tpy)_2]^{1-}$. *Inorg. Chem*. **2012**, *51*, 3718−3732.

[56] Wang, M.; England, J.; Weyhermüller, T.; Kokatam, S.-L.; Pollock, C. J.; DeBeer, S.; Shen, J.; Yap, G. P. A.; Theopold, K. H.; Wieghardt, K. New Complexes of Chromium(III) Containing Organic π-Radical Ligands: An Experimental and Density Functional Theory Study. *Inorg. Chem*. **2013**, *52*, 4472−4487.

[57] Scarborough, C. C.; Sproules, S.; Doonan, C. J.; Hagen, K. S.; Weyhermüller, T.; Wieghardt, K. Scrutinizing Low-Spin Cr(II) Complexes. *Inorg. Chem*. **2012**, *51*, 6969−6982.

[58] Banerjee, P.; Sproules, S.; Weyhermüller, T.; DeBeer George, S.; Wieghardt, K. Electronic Structure of the [Tris(dithiolene)chromium]^{z} (z = 0, 1−, 2−, 3−) Electron Transfer Series and Their Manganese(IV) Analogues. An X-ray Absorption Spectroscopic and Density Functional Theoretical Study. *Inorg. Chem.* **2009**, *48*, 5829–5847.

[59] Yuan, R.; Ren, G.; Mahmood, Q.; Zeng, Y.; Wang, Y.; Liang, T.; Sun, W.H. Cycloheptyl-Fused Iminopyridine-Iron Catalysts for Isoprene Polymerization with Enhanced Activity and Thermal Stability. *Organometallics* **2023**, *42*, 3307–3318.

[60] Brienne, S. H. R.; Boyd, P. D. W.; Schwerdtfeger, P.; Bowmaker, G. A.; Cooney, R. P. Intensity Enhancements in the IR Spectra of Organic Radical Ions. A Theoretical Study. *J. Chem. Soc. Faraday Trans*. **1993**, *89*, 3015–3020.

[61] Zamadar, M.; Asaoka, S.; Grills, D. C.; Miller, J. R. Giant infrared absorption bands of electrons and holes in conjugated molecules. *Nat. Commun*. **2013**, *4*, 2818.

[62] Zhu, G.; Zhang, X.; Zhao, M.; Wang, L.; Jing, C.; Wang, P.; Wang, X.; Wang, Q. Influences of Fluorine Substituents on Iminopyridine Fe(II)- and Co(II)-Catalyzed Isoprene Polymerization. *Polymers* **2018**, *10*, 934.

[63] Zhang, T.; Guo, D.; Jie, S.; Sun, W. H.; Li, T.; Yang, X. Influence of electronic effect on catalytic activity of salicylaldiminato nickel(II) complexes. *J. Polym. Sci. A* **2004**, *42*, 4765−4774.

[64] Zanchin, G.; Pierro, I.; Parisini, E.; Martí-Rujas, J.; Ricci, G.; Leone, G. Synthesis, structure and behavior of vanadium(III) diphosphine complexes in the homo- and co-polymerization of ethylene with norbornene: the ligand donor strength and bite angle make the difference. *J. Organomet. Chem.* **2018**, *861*, 142−150.

[65] Chi, M. J.; Chen, A.; Tan, C.; Chen, C. Positional Electronic Effects in Iminopyridine-N-oxide Nickel Catalyzed Ethylene Polymerization. *Chinese J. Chem*. **2021**, *39*, 1683−1689.

[66] He, F.; Wang, D.; Jiang, B.; Zhang, Z.; Cheng, Z.; Fu, Z.; Zhang, Q.; Fan, Z. Introducing electron-donating substituents on ligand backbone of α-diimine nickel complex and the effects on catalyst thermal stability in ethylene polymerization. *Inorg. Chim. Acta* **2019**, *486*, 704−710.

[67] Zanchin, G.; Bertini, F.; Vendier, L.; Ricci, G.; Lorber, C.; Leone, G. Copolymerization of ethylene with propylene and higher α-olefins catalyzed by (imido)vanadium(IV) dichloride complexes. *Polym. Chem.* **2019**, *10*, 6200−6216.

[68] Wang, C.; Kang, X.; Dai, S.; Cui, F.; Cui, F.; Li, Y.; Mu, H.; Mecking, S.; Jian, Z. Efficient Suppression of Chain Transfer and Branching via C_s-Type Shielding in a Neutral Nickel(II) Catalyst. *Angew. Chem*. **2021**, *133*, 4064 –4068.

[69] Zhang, W.; Sun, W. H.; Zhang, S.; Hou, J.; Wedeking, K.; Schultz, S.; Fröhlich, R.; Song, H. Synthesis, Characterization, and Ethylene Oligomerization and Polymerization of [2,6-Bis(2-benzimidazolyl)pyridyl]chromium Chlorides. *Organometallics* **2006**, *25*, 1961−1969.